Journal of Materials Chemistry A

PAPER

View Article Online
View Journal | View Issue

Cite this: J. Mater. Chem. A, 2016, 4, 14804

Parallel bulk heterojunction photovoltaics based on all-conjugated block copolymer additives†

Jorge W. Mok,[a] Dylan Kipp,[b] Luis R. Hasbun,[a] Andrei Dolocan,[c] Joseph Strzalka,[d] Venkat Ganesan*[b] and Rafael Verduzco*[ae]

Received 29th July 2016
Accepted 23rd August 2016

DOI: 10.1039/c6ta06502c

www.rsc.org/MaterialsA

In recent studies, we demonstrated that the addition of block copolymers to binary donor–acceptor blends represents an effective approach to target equilibrium, co-continuous morphologies of interpenetrating donors and acceptors. Here, we report a study of the impact of all-conjugated poly(thieno[3,4-*b*]-thiophene-*co*-benzodithiophene)-*b*-polynaphthalene diimide (PTB7-*b*-PNDI) block copolymer additives on the electronic properties and photovoltaic performance of bulk heterojunction organic photovoltaic active layers comprised of a PTB7 donor and a phenyl-C_{61}-butyric acid methyl ester ($PCBM_{61}$) acceptor. We find that small amounts of BCP additives lead to improved performance due to a large increase in the device open-circuit voltage (V_{OC}), and the V_{OC} is pinned to this higher value for higher BCP additive loadings. Such results contrast prior studies of ternary blend OPVs where either a continuous change in V_{OC} or a value of V_{OC} pinned to the lowest value is observed. We hypothesize and provide evidence in the form of device and morphology analyses that the impact of V_{OC} is likely due to the formation of a parallel bulk heterojunction made up of isolated PCBM and PNDI acceptor domains separated by intermediate PTB7 donor domains. Altogether, this work demonstrates that all-conjugated block copolymers can be utilized as additives to both dictate morphology and modulate the electronic properties of the active layer.

Introduction

Bulk heterojunction (BHJ) organic photovoltaic (OPV) devices are comprised of an interpenetrating network of donor and acceptor semiconductors. Systematic materials design and processing optimization has produced tremendous progress in device performance, and recent studies have reported single-junction device efficiencies exceeding 10%.[1,2] However, a key challenge in further development of these devices is finding reliable strategies for controlling and directing the blend morphologies, which exert a significant impact on the electronic properties, stability, mechanical robustness, and overall functionality. A number of strategies have been implemented to optimize and control the nanoscale active layer morphology, including the use of processing additives, solvent annealing, surface treatment, and others, as detailed in recent reviews and studies.[3–13]

The use of block copolymer additives represents an effective approach to control the donor–acceptor morphology. Indeed, properly designed block copolymer additives can be utilized to improve thermal stability and potentially produce equilibrium, bicontinuous phases of interpenetrating donor and acceptor semiconductors. As detailed in recent reviews, a number of studies have reported the design and implementation of conjugated block copolymers in bulk heterojunction active layers and demonstrated clear benefits to using BCP additives.[14–17] For example, Chen *et al.* studied poly(3-hexylthiophene)-*b*-poly(ethylene oxide) (P3HT-*b*-PEO) additives and found that these additives could be used to tune domain sizes in thermally annealed OPVs.[18] Sun *et al.* reported P3HT-*b*-polystyrene (PS) additives that had a beneficial impact on stability, crystallinity, and photovoltaic performance.[19] Kim *et al.* reported P3HT additives with poly(4-vinylpyridine) (P4VP) side-chains that improved thermal stability.[20] However, a limitation of these prior studies is that they have focused primarily on block copolymers with optically and electronically inactive polymer blocks or backbones, which can be detrimental to electronic properties, especially at higher loadings. Furthermore, these studies have focused predominantly on BHJ OPVs

[a]Department of Chemical and Biomolecular Engineering, Rice University, Houston, Texas 77005, USA. E-mail: rafaelv@rice.edu
[b]Department of Chemical Engineering, The University of Texas at Austin, Austin, Texas 78712, USA. E-mail: venkat@che.utexas.edu
[c]Department of Materials Science and Texas Materials Institute, University of Texas at Austin, Austin, Texas 78712, USA
[d]X-ray Science Division, Advanced Photon Source, Argonne National Laboratory, Argonne, Illinois 60439, USA
[e]Department of Materials Science and NanoEngineering, Rice University, Houston, Texas 77005, USA

† Electronic supplementary information (ESI) available: Experimental details, average values for device characteristics, ^{1}H NMR spectra of polymers, TEM images of ternary blends, and GIWAXS data for ternary blends. See DOI: 10.1039/c6ta06502c

with P3HT as the donor, while there is still less clarity on effects expected in BHJ OPVs based on the more recently explored non-crystalline, alternating copolymers as the donor.

Fully conjugated block copolymers with donor and acceptor blocks can be utilized as additives to both modulate the morphology and potentially improve the electronic properties of the active layer. However, only a few studies have investigated all-conjugated BCPs as additives to BHJ OPVs. Mulherin *et al.* demonstrated that all-conjugated BCP additives could suppress phase separation at 40 wt% loadings.[21] Lee *et al.* found that all-conjugated BCP additives improved the performance of P3HT/phenyl-C_{61}-butyric acid methyl ester ($PCBM_{61}$) BHJ OPVs.[22] Recently, we investigated the morphological impact of fully conjugated block copolymers as additives for dictating the morphology of poly(thieno[3,4-*b*]-thiophene-*co*-benzodithiophene) (PTB7) bulk heterojunction OPVs. We applied a combined simulation and experiment-based approach to investigate if block copolymer (BCP) additives can be used to intelligently control the self-assembled morphologies of PTB7/$PCBM_{61}$ mixtures. Single chain in mean field (SCMF) simulations[23,24] were used to identify regions within the PTB7/PCBM phase diagram where all-conjugated poly(thieno[3,4-*b*]-thiophene-*co*-benzodithiophene)-*b*-poly(naphthalene diimide) (PTB7-*b*-PNDI) block copolymer (BCP) additives would lead to co-continuous equilibrium morphologies desired for photovoltaic applications. These simulations predicted the formation of co-continuous phases at much higher block copolymer additive concentrations than that is typically studied (>40 wt%), and TEM and X-ray diffraction analysis of blend films produced qualitative agreement with computational predictions.[25] In a subsequent study, we followed up with more detailed SCMF simulations that provided design rules for producing bicontinuous phases with BCP compatibilizers.[26] These studies demonstrate that all-conjugated block copolymer additives are useful for dictating the morphology of BHJ OPVs, but the impact of these additives on electronic properties and performance is unclear.

Here, we report a study of the impact of all-conjugated PTB7-*b*-PNDI block copolymer additives on the electronic properties and photovoltaic performance of bulk heterojunction OPV active layers comprised of a PTB7 donor and a $PCBM_{61}$ acceptor. We find that small amounts of BCP additives lead to a large increase in the device open-circuit voltage (V_{OC}), and the V_{OC} is pinned to this higher value for higher BCP additive loadings. By comparison, PNDI homopolymer additives produce a continuous increase in V_{OC} with increasing loading. We hypothesize and provide evidence in the form of device and morphology analyses that the impact of V_{OC} is due to the formation of a parallel bulk heterojunction[27,28] made up of isolated PCBM-rich and PNDI-rich acceptor domains separated by intermediate PTB7 donor domains. Altogether, this work demonstrates that all-conjugated block copolymers can be utilized as additives to both dictate morphology and modulate the electronic properties of the active layer and may represent a novel approach for producing BHJ OPVs with enhanced V_{OC}.

Experimental details

Materials

4,9-Dibromo-2,7-bis(2-octyldodecyl)benzo[*lmn*][3,8]phenanthroline-1,3,6,8(2*H*,7*H*)-tetraone, 2-ethylhexyl-4,6-dibromo-3-fluorothieno[3,4-*b*]thiophene-2-carboxylate, and 2,6-bis(trimethyltin)-4,8-bis(2-ethylhexyloxy)benzo[1,2-*b*:4,5-*b*′] were purchased from Sunatech Inc. All other reagents were purchased from commercial sources and used as received.

Materials synthesis

PTB7 (Scheme 1). 2-Ethylhexyl-4,6-dibromo-3-fluorothieno[3,4-*b*]thiophene-2-carboxylate (260 mg, 0.56 mmol), 2,6-bis(trimethyltin)-4,8-bis(2-ethylhexyloxy)benzo[1,2-*b*:4,5-*b*′] (430 mg, 0.56 mmol), and tetrakis-(triphenylphosphine)-palladium(0) ($Pd(PPh_3)_4$) (25 mg) were added to a microwave reaction tube and transferred to a glovebox where anhydrous chlorobenzene (5 mL) was added. The reaction tube was transferred to a microwave reactor, where the polymerization proceeded at 180 °C for 1 hour. The polymer was precipitated in 300 mL of cold methanol, and further purified by washing in a Soxhlet extractor with methanol and acetone before collecting separate fractions in hexane and chloroform. The low molecular-weight hexane fraction was concentrated and precipitated in cold methanol and dried under vacuum overnight and further used for the synthesis of the PTB7-*b*-PNDI. The high molecular weight chloroform fraction was concentrated and precipitated in cold methanol and dried under vacuum overnight. ^{1}H NMR ($CDCl_3$, 400 MHz): δ 0.80–2.40 (45H, br), 3.90–4.70 (6H, br), 7.00–7.90 (2H, br). GPC (hexanes fraction): M_w = 11.6 kDa and PDI = 1.9. (Chloroform fraction): M_w = 26.2 kDa, PDI = 2.6, DP = 33, and yield = 40%.

PNDI (Scheme 2). 4,9-Dibromo-2,7-bis(2-octyldodecyl)benzo[*lmn*][3,8]phenanthroline-1,3,6,8(2*H*,7*H*)-tetraone (510 mg, 0.52 mmol), 5,5′-bis(trimethylstannyl)-2,2′-bithiophene (250 mg, 0.52 mmol), tris(dibenzylideneacetone) dipalladium(0) (15 mg, 14.67 μmol), and tri(*o*-tolyl)phosphine (12 mg, 5.88 μmol) were added to a microwave reaction tube and transferred to a glovebox where anhydrous toluene (10 mL) was added. The sealed reaction tube was transferred to a microwave reactor, where the polymerization proceeded at 180 °C for 1 hour. The polymer was precipitated in 300 mL of cold methanol, and further purified by washing in a Soxhlet extractor with acetone and hexane, and then collected in chloroform. The chloroform fraction was concentrated and precipitated in cold methanol and dried under vacuum overnight. ^{1}H NMR ($CDCl_3$, 400 MHz): δ 0.80–0.90 (12H, br), 1.20–1.40 (64H, br), 4.10–4.12 (4H, br), 8.95 (2H, s). GPC: M_w = 59.8 kDa, PDI = 5.4, DP = 60, yield = 80%.

PTB7-*b*-PNDI (Scheme 3). PTB7 (M_w = 11.6 kDa and PDI = 1.9) (132 mg, 6.16 μmol), 4,9-dibromo-2,7-bis(2-octyldodecyl)benzo[*lmn*][3,8]phenanthroline-1,3,6,8(2*H*,7*H*)-tetraone (120 mg, 0.12 mmol), 5,5′-bis(trimethylstannyl)-2,2′-bithiophene (60 mg, 0.12 mmol), tris(dibenzylideneacetone) dipalladium(0) (5 mg, 4.89 μmol), and tri(*o*-tolyl)phosphine (6 mg, 1.96 μmol) were added to a microwave reaction tube and transferred to a glovebox where anhydrous chlorobenzene (4 mL) was added. The reaction

tube was transferred to a microwave reactor, where the polymerization proceeded at 180 °C for 1 hour. The polymer was precipitated in 300 mL of cold methanol, and further purified by washing in a Soxhlet extractor with methanol, acetone, and hexanes and collected in chloroform. The chloroform fraction was concentrated and precipitated in cold methanol and dried under vacuum overnight. The PTB7 weight fraction was determined by comparing the integrated areas of peaks at 7.50–7.90 ppm (PTB7, 2H) and 8.00–8.84 ppm (PNDI, 2H). ^{1}H NMR ($CDCl_3$, 400 MHz): δ 0.80–2.40 (123H, br), 3.90–4.70 (8H, br), 7.50–7.90 (2H, br), 8.00–8.84 (2H, br). GPC: M_w = 47.1 kDa, PDI = 3.0, and yield = 70%. PTB7 wt% = 9.7%.

^{1}H NMR analysis of all synthesized materials is provided in ESI Fig. S1–S3.†

Results and discussion

The majority of all-conjugated block copolymers are comprised of one or more polythiophene blocks,[29–32] in which the polythiophene block can be synthesized by controlled catalyst transfer polycondensation.[33–35] Here, we target a conjugated block copolymer comprised of two alternating copolymers, PTB7 and PNDI (Scheme 4). Our overall approach to the synthesis of PTB7-*b*-PNDI block copolymers involves sequential Stille polycondensation reactions along with purification of reactive intermediates and the final product through selective solvent extraction. First, PTB7 was synthesized in a Stille polycondensation reaction followed by fractionation by solvent washing in a Soxhlet extractor. Low and high PTB7 molecular weight fractions were collected by washing with hexanes and chloroform, respectively. Next, a PTB7-*b*-PNDI block copolymer was synthesized in a Stille polycondensation reaction in the presence of PTB7 macroreagent from the low molecular weight fraction extracted from the first step. After polymerization, the final material was washed in a Soxhlet reactor to remove oligomers and unreacted PTB7 macroreagent before collecting in chloroform.

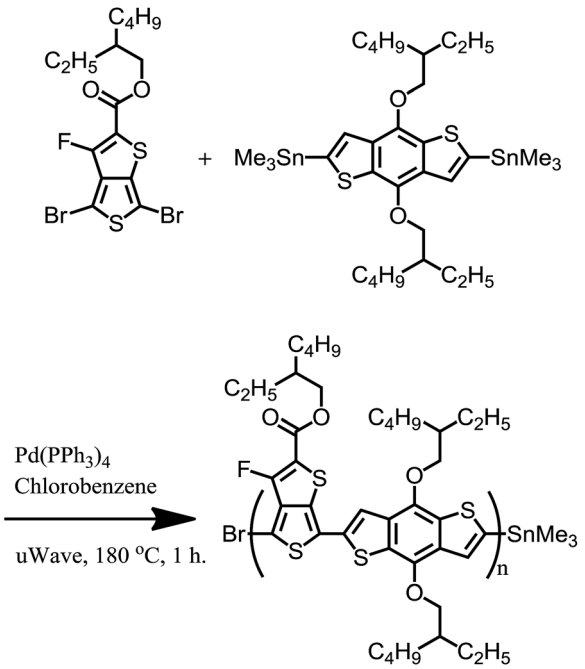

Scheme 1 Synthetic scheme for the preparation of PTB7.

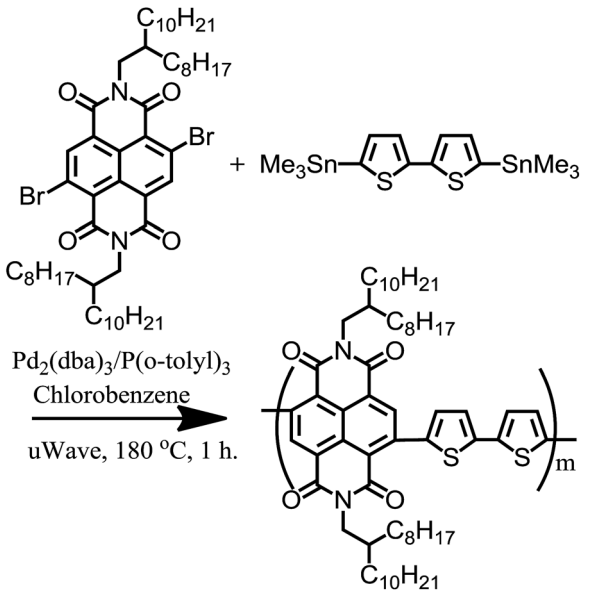

Scheme 2 Synthetic scheme for the preparation of PNDI.

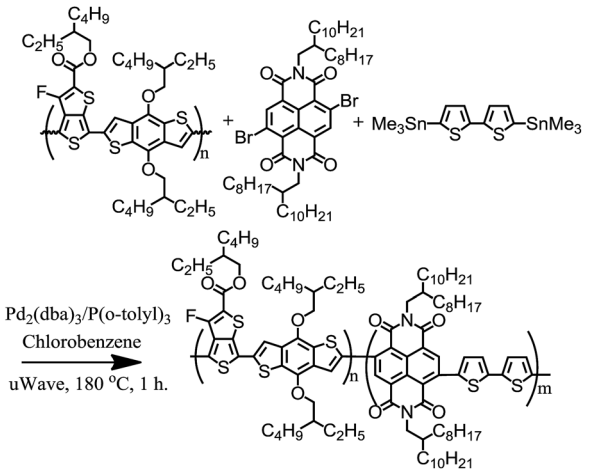

Scheme 3 Synthetic scheme of PTB7-*b*-PNDI.

The molecular weight, composition, and polydispersity of the PTB7-*b*-PNDI block copolymer along with PTB7 and PNDI homopolymers were determined through a combination of size exclusion chromatography (SEC) (Fig. 1), ^{1}H NMR (ESI Fig. S1–S3†), and steady state UV-Vis absorbance spectroscopy (ESI Fig. S4†), and are tabulated in Table 1. SEC analysis shows a clear shift to shorter retention times for the final block copolymer product, and ^{1}H NMR analysis confirms the presence of both PTB7 and PNDI in the final product. Time of flight secondary ion mass spectroscopy (TOF-SIMS) also shows evidence of both PTB7 and PNDI in the final product, as shown

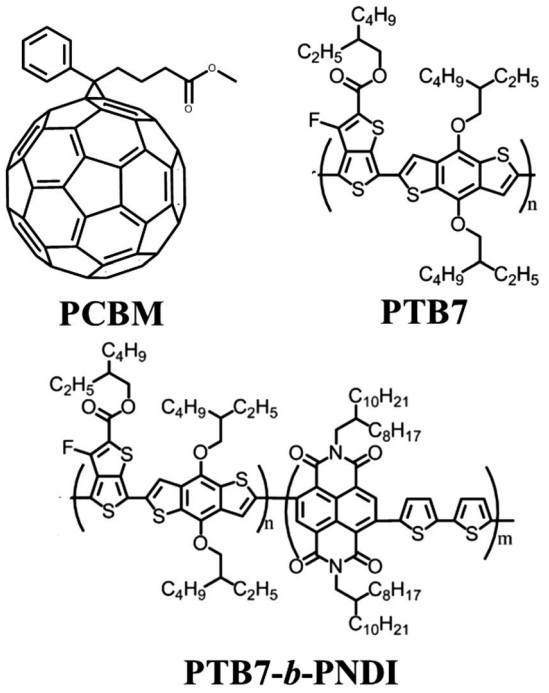

Scheme 4 Structures of the PTB7 donor, PCBM acceptor, and all-conjugated PTB7-*b*-PNDI block copolymer additive.

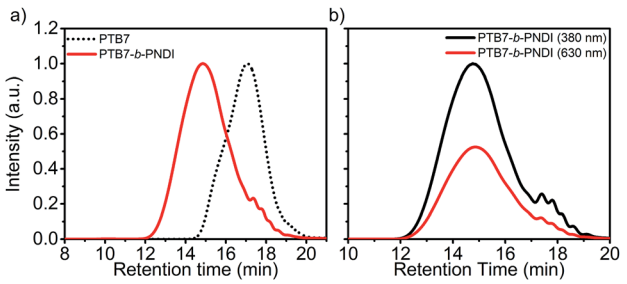

Fig. 1 (a) Size exclusion chromatography (SEC) traces of PTB7 and PTB7-*b*-PNDI with (a) differential refractive index analysis and (b) UV-VIS analysis at 380 nm and 680 nm, corresponding to peak absorbances for PNDI and PTB7, respectively.

in ESI Fig. S5.† Although the presence of some PNDI homopolymers cannot be excluded due to the overlap in the distributions, little or no PTB7 macro-reagent is present in the final product. SEC-UV-VIS analysis shows coincident peaks at both 380 and 630 nm, corresponding to peak absorbances for PNDI and PTB7 blocks, respectively, and greater absorbance intensity at 630 nm is observed for the block copolymer relative to the PNDI homopolymer. Based on ^{1}H NMR analysis, the PTB7-*b*-PNDI block copolymer is comprised of 9.7 wt% PTB7 (see ESI† for details on analysis). Two additional estimates of the block copolymer composition are provided in the ESI† based on (i) SEC UV-Vis analysis (estimated composition 9.9 wt% of PTB7) and (ii) steady state solution UV-Vis absorption (estimated composition 9.5 wt% of PTB7). All three methods estimate comparable composition of the block copolymer. The discrepancy between the M_w of the initial PTB7 macro-reagent (11.6 kg mol^{-1}) and that of the PTB7 block in the final block copolymer (approx. 5 kg mol^{-1}) suggests fractionation during the second Stille polycondensation reaction. Lower molecular weight PTB7 macroreagent reacts faster, as would be expected, and unreacted PTB7 is washed out in the subsequent sample purification.

Next, we examined the impact of PTB7-*b*-PNDI additives on the performance and electronic properties of PTB7/PCBM$_{61}$ bulk heterojunction photovoltaic devices. The overall device architecture consisted of an inverted structure (ITO/ZnO/active layer/PEDOT:PSS/Ag), and the overall ratio between PTB7 and PCBM$_{61}$ was held constant at 1 : 1.75 consistent with prior optimization studies of PTB7/PCBM$_{61}$ OPVs.[11,36] Fig. 2 shows current–voltage (*J*–*V*) curves for devices ranging from 0 to 15 wt% block copolymer added, and Table 2 provides quantitative data for the best performance for each blend. Device characteristics averaged over 10 devices exhibit similar trends and are provided in ESI Table S1.† The PCE measured for the base case of PTB7/PCBM$_{61}$ with no additive is comparable to prior literature reports which use PCBM$_{61}$ as the acceptor.[11,36]

A significant improvement of PCE was observed with small amounts of BCP additives, from a PCE of 3.05% with no additive up to 5.1% with 3 wt% BCP additive. Most striking is the increase in the V_{OC} with the addition of BCPs, from a value of 0.72 V to 0.82 V with only 2 wt% BCP added. The V_{OC} remains constant at 0.82 V for higher contents of BCP beyond 2 wt%.

Table 1 Molecular weight, polydispersities and composition of polymers

Polymer	M_w[a] (kg mol^{-1})	M_n[a] (kg mol^{-1})	PDI[a]
PTB7 – 1	11.6	6.2	1.9
PTB7 – 2	26.2	10.1	2.6
PTB7-*b*-PNDI[b]	47.1	15.8	3.0
PNDI	59.8	11.1	5.4

[a] Measured by SEC relative to monodisperse PS standards. [b] PTB7-*b*-PNDI is comprised of 9.7 wt% PTB7 (12 mol%).

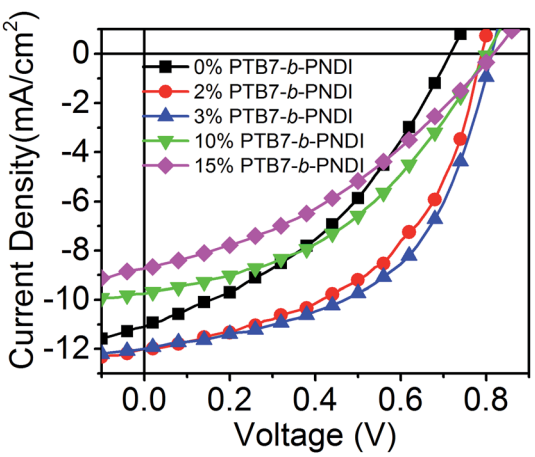

Fig. 2 *J*–*V* curves of photovoltaic devices with PTB7-*b*-PNDI additives illuminated at AM 1.5 and 100 mW cm^{-2}.

Table 2 Device characteristics of PTB7/$PCBM_{61}$ OPVs with additives. Best cell characteristics reported, average device characteristics provided in the ESI. Active layer thickness: 70 nm[a]

Additive	Additive conc. (wt%)	PCE (%)	V_{OC} (V)	J_{SC} (mA cm^{-2})	FF (%)
No additive	0	3.1	0.72	10.9	38.9
PTB7-*b*-PNDI	1	4.2	0.76	12.3	44.6
	2	5.0	0.82	12.1	50.6
	3	5.1	0.82	11.9	52.5
	10	3.3	0.82	9.7	41.4
	15	2.2	0.82	9.3	29.9
PNDI	2	5.2	0.76	16.0	43.1
	3	4.5	0.78	15.1	40.3
	5	3.1	0.78	9.7	40.6
	10	2.7	0.80	8.8	38.4
	15	2.7	0.84	9.3	34.5

[a] PCE: power conversion efficiency; J_{SC}: short circuit current; V_{OC}: the open-circuit voltage; FF: fill factor.

This value of V_{OC} is also higher than that reported for state-of-the art PTB7–$PCBM_{61}$ and PTB7–$PCBM_{71}$ OPV devices,[5,37,38] including studies that incorporate a third component to enhance performance.[39–43] A recent study by Lu *et al.* found a similar magnitude increase in V_{OC} with the addition of 50 wt% of a second donor.[43] Importantly, the observed trend of V_{OC} is different from that typically observed for ternary blend systems, where a number of studies have reported either a linear change in V_{OC} for blends with good compatibility or pinning of V_{OC} to a low value for blends with poor compatibility.[43–45] Here, we observe pinning of V_{OC} to a higher value. The short-circuit current (J_{SC}) and fill factor (FF) increase with the added BCP and then quickly drop for BCP contents above 10 wt%.

To further understand the impact the BCP additive has on electronic properties, we analyzed ternary PTB7/$PCBM_{61}$/PNDI ternary blend OPVs. With a pure PNDI additive, the V_{OC} exhibited a roughly linear increase with increasing additive concentration. The PNDI additive has a beneficial impact on device PCE predominantly through an increase in the short-circuit current and fill factor. The evolution of device characteristics with the PNDI additive was consistent with prior studies of ternary blend OPVs with two acceptors.[46]

Trends in device characteristics with different additive contents are shown in Fig. 3. The results shown for PTB7-*b*-PNDI and PNDI homopolymer additives reveal a qualitative and quantitative difference in the impact these additives have on V_{OC} and J_{SC}. The PTB7-*b*-PNDI additive has a dramatic impact on V_{OC}, which reaches a plateau at 2 wt% and remains high for subsequent devices. In contrast, the V_{OC} increases more gradually with the PNDI additive, eventually reaching a value of 0.82 V at 15 wt% additive, and PNDI additive has a more dramatic impact on the J_{SC}.

There are several examples reported in the literature in which the V_{OC} is pinned to the lowest value V_{OC} due to poor compatibility between components, and, for example, varying the additive concentration from 0 to 90% does not change the

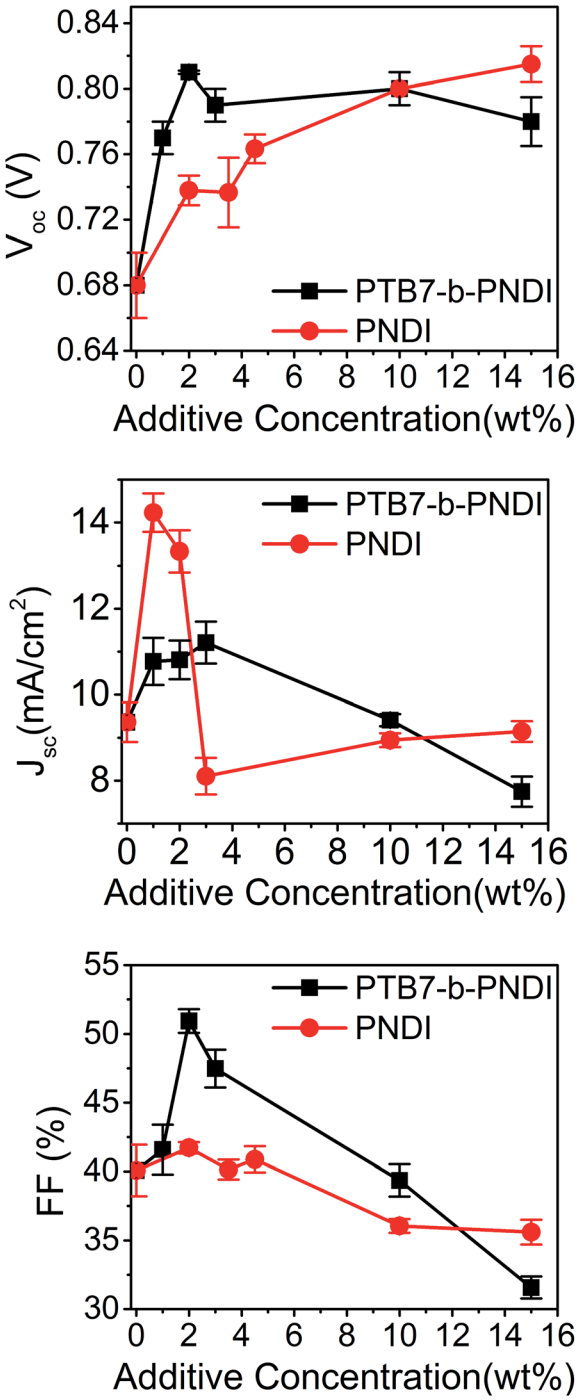

Fig. 3 Device characteristics of PTB7/$PCBM_{61}$/additive ternary blend cells as a function of additive composition. Averaged over 10 devices.

V_{OC}.[44,45] In one example, Khlyabich *et al.* examined ternary blend OPVs comprised of two immiscible polymeric donors and found a low V_{OC} pinned by the smallest HOMO of the two polymer donors and the LUMO of the acceptor.[45] Lu *et al.* studied ternary blends of PTB7 a second donor polymer poly-3-oxothieno[3,4-*d*]isothiazole-1,1-dioxide/benzodithiophene (PID2) and $PCBM_{71}$. EQE measurements showed improved light harvesting by PID2, enhancing PCE from 7.2% to 8.2% at optimal additive composition. However, V_{OC} was pinned at 0.72

V for blend compositions up to 90% PID2, compared to 0.86 V for 100% PID2 as a donor.[39] Here, in the case of PTB7-*b*-PNDI additives, we observe an increased V_{OC} compared to that in the case of both PNDI-*b*-PTB7 and PNDI additives.

Given the relative ordering of the energy levels (see Fig. 4), and the electron affinity of PNDI,[47–49] PNDI is expected to act as an electron acceptor (see ESI Fig. S6† for cyclic voltammetry measurements). This leads to the possibility that PNDI and $PCBM_{61}$ form an alloyed acceptor blend.[46] However, in the case of PTB7-*b*-PNDI the V_{OC} is observed to be independent of composition above 2 wt% PTB7-*b*-PNDI. Furthermore, while devices with the pure PNDI additive show a continuous change in V_{OC} which may reflect an alloyed acceptor, the change in V_{OC} is larger than would be expected for just 15 wt% PNDI added, where the $PCBM_{61}$ should still be dominant. Instead, the observed device characteristics are consistent with a parallel-type model proposed for ternary blend OPVs.[27,28] In this picture, the third component forms a phase-segregated percolating channel rather than blending or alloying with the donor or acceptor phase.

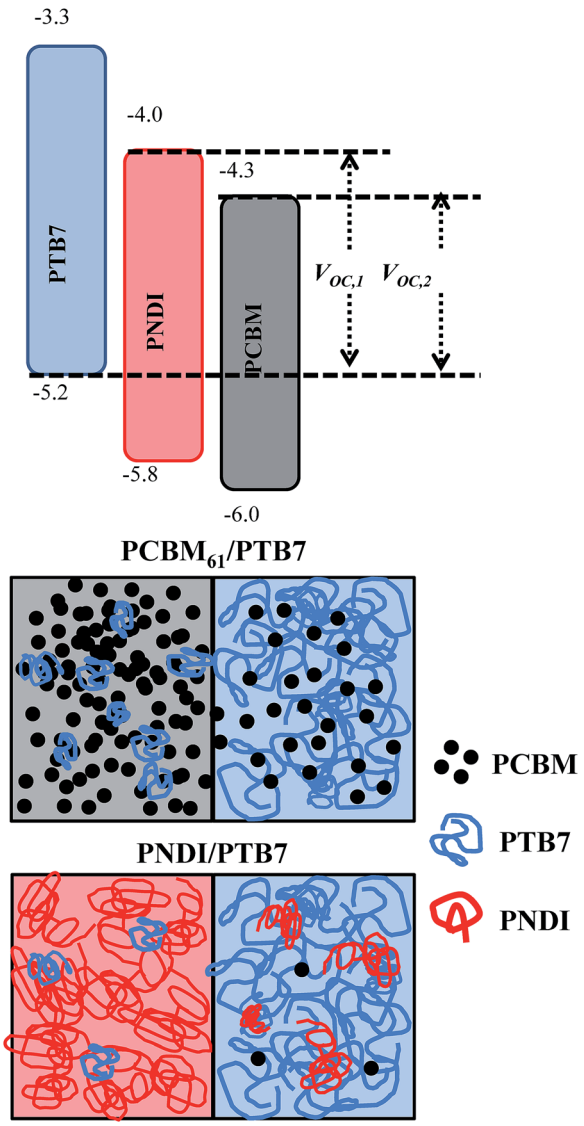

Fig. 4 (Top) Energy level diagram for ternary blend OPVs and (bottom) schematic of domain interfaces for BHJ OPVs. Without any additive, the only domains are a $PCBM_{61}$-rich and PTB7-rich domain. With the PNDI additive (PTB7-*b*-PNDI or PNDI homopolymer) phase segregated PNDI domains form a separate channel for electron collection and transport. For clarity, no mixing is shown between PNDI and $PCBM_{61}$.

To understand the predictions of this model for the particular system under study, we first note that the energy levels of PNDI are such that the HOMO and LUMO are positioned between those of PTB7 and PCBM, as shown in Fig. 4. In a perfectly mixed system, electrons would relax to the lowest energy state available, which would be either on PCBM or on an alloy of PCBM and PNDI. In the parallel-like model, with the addition of PTB7-*b*-PNDI, PNDI forms an independent percolating channel. As a result, the electrons can distribute to the LUMO of PNDI, resulting in the observed increase in the V_{OC}.

Surface energy values provide an estimate of enthalpic interactions between different components and can provide insight into the expected morphological changes. The surface energies were previously measured through contact angle measurements and can used to estimate the enthalpic interactions between different components.[25] The surface energies of the polymers and binary Flory–Huggins interaction parameters χ indicate that PNDI will be strongly segregated from both PTB7 and PCBM ($\chi_{PTB7-PNDI} = 1.20$ and $\chi_{PCBM-PNDI} = 3.36$), while mixing is expected between PTB7 and $PCBM_{61}$ ($\chi_{PTB7-PCBM} = 0.77$), as has been observed in prior morphological studies.[5,11] As a result, PNDI should be segregated from both PTB7 and $PCBM_{61}$, consistent with the expected morphology of a parallel-like BHJ OPV.[27,28]

For comparison with parallel bulk heterojunction photovoltaics, we fabricated true parallel bilayer OPVs. Bilayer OPVs provide a useful model system for studying electronic properties of the donor–acceptor interface.[50] Bilayer devices with $PCBM_{61}$/PTB7 or PNDI/PTB7 active layers were fabricated separately and then connected in parallel, as shown in ESI Fig. S7.† The device characteristics and *J*–*V* curves are shown in ESI Table S2 and Fig. S7.† The PTB7/$PCBM_{61}$ bilayer device exhibits a V_{OC} of 0.72 V while the PTB7/PNDI device has a much higher V_{OC} of 0.80 V. When connected in parallel, the resulting V_{OC} is 0.74 V, intermediate between the two bilayer devices and in good agreement with the expected V_{OC} based on weighting each cell by its current production.[28] Similarly, the parallel bulk heterojunction OPVs exhibit an increase in V_{OC} with the addition of block copolymers. The higher value of V_{OC} in the block copolymer devices indicates a larger current through the PNDI domains relative to the parallel bilayer OPVs.

To investigate phase separation and mixing in the ternary blend system, we analyzed model bilayer blends of PTB7, PNDI, and deuterated $PCBM_{61}$ (d-$PCBM_{61}$) by time of flight secondary ion mass spectroscopy (TOF-SIMS). TOF-SIMS has been applied to organic and inorganic films to perform compositional and isotopic analyses along with depth profiling with subnanometer resolutions.[51–53] We analyzed bilayer films in order to investigate mixing and phase separation of d-PCBM from either PNDI or PTB7, as shown schematically in Fig. 5. d-$PCBM_{61}$ was used in

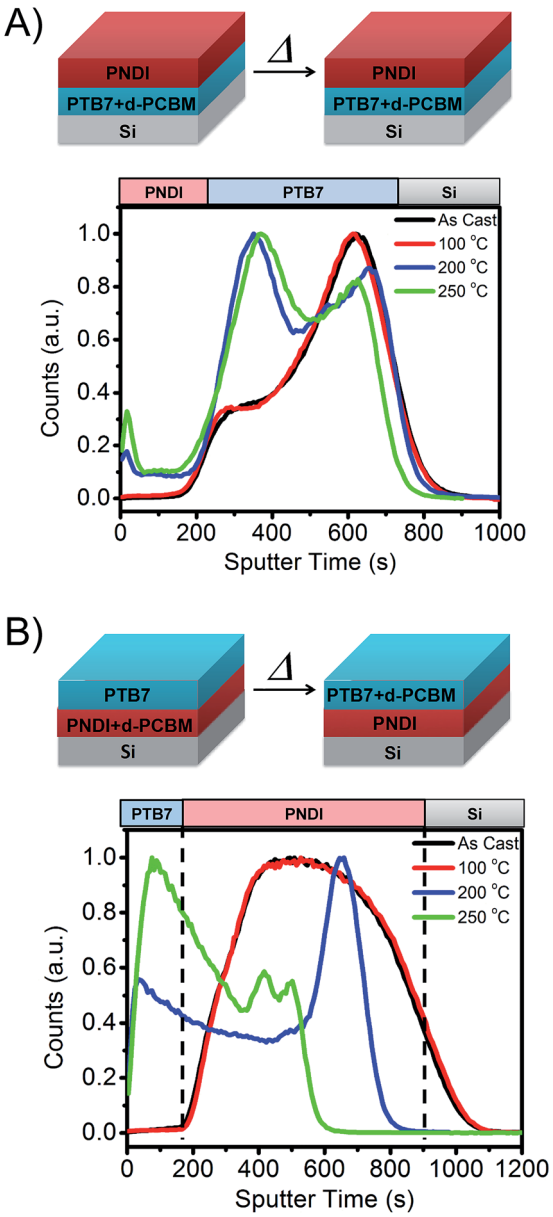

Fig. 5 Schematics and TOF-SIMS analysis of $^{2}H^{-}$ distribution in bilayer films of (A) pure PNDI on top of a PTB7/d-PCBM blend and (B) pure PTB7 on top of a PNDI/d-PTB7 blend. The $^{2}H^{-}$ distribution corresponds to d-$PCBM_{61}$ in the films. Samples were annealed at 100 °C, 200 °C and 250 °C for 10 minutes.

place of $PCBM_{61}$ to enable compositional analysis through detection of ^{2}H ions.

In one experiment, a film of pure PNDI (70 nm) was deposited on top of a blend film (50 : 50 wt%) of PTB7:d-$PCBM_{61}$ while in a second experiment a film of pure PTB7 (70 nm) was deposited on top of a blend film (50 : 50 wt%) of PNDI and d-$PCBM_{61}$. The bilayers were prepared through film transfer at room temperature, ensuring that no mixing occurred prior to TOF-SIMS analysis and/or thermal annealing. Based on the interaction energies of each component, we hypothesized that d-$PCBM_{61}$ would preferentially segregate to the PTB7 layer. In the first experiment, we thus expected d-$PCBM_{61}$ to remain in the bottom PTB7 layer, while in the second experiment we expected diffusion of the d-$PCBM_{61}$ to the top PTB7 layer during annealing. Due to the slow diffusion kinetics and incompatibility between PTB7 and PNDI, no mixing was expected during annealing. Indeed, this is supported through TOF-SIMS analysis of secondary ions corresponding to each component (see ESI Fig. S8†).

As shown in Fig. 5B, d-$PCBM_{61}$ remains in the PTB7 layer even after annealing up to a temperature of 250 °C. Some diffusion of $PCBM_{61}$ is observed towards the PNDI interface, but d-$PCBM_{61}$ remains distributed only within the PTB7 film. In contrast, for the case where d-$PCBM_{61}$ and PNDI are initially blended, segregation of d-$PCBM_{61}$ to the top PTB7 film is indeed observed. The d-$PCBM_{61}$ is initially broadly distributed within the bottom layer, and after annealing at 200 °C segregation towards the PTB7 and the bottom Si interface is observed. On annealing at a higher temperature of 250 °C, most of the d-$PCBM_{61}$ is located within the PTB7 domain. TOF-SIMS analysis thus demonstrates that the PNDI will segregate strongly from both PTB7 and $PCBM_{61}$ domains.[25]

To quantify morphological changes within bulk-heterojunction OPVs, ternary blend films were analyzed by transmission electron microscopy (TEM) and grazing-incidence wide angle X-ray scattering (GIWAXS). TEM and GIWAXS samples were prepared under similar conditions to those of devices, by spin-coating blends from a mixture of chlorobenzene : DIO (97 : 3 v/v) and annealing at 100 °C for 10 minutes. TEM results suggest that, indeed, a layer of PTB7 may insulate the PNDI from the PCBM (Fig. 6 and ESI Fig. S9†). The TEM analysis of PTB7:$PCBM_{61}$ blends is shown in ESI Fig. S10† for reference. In the TEM micrographs for blends with PTB7-*b*-PNDI and PNDI additives, we observe evidence of three-phase coexistence: black

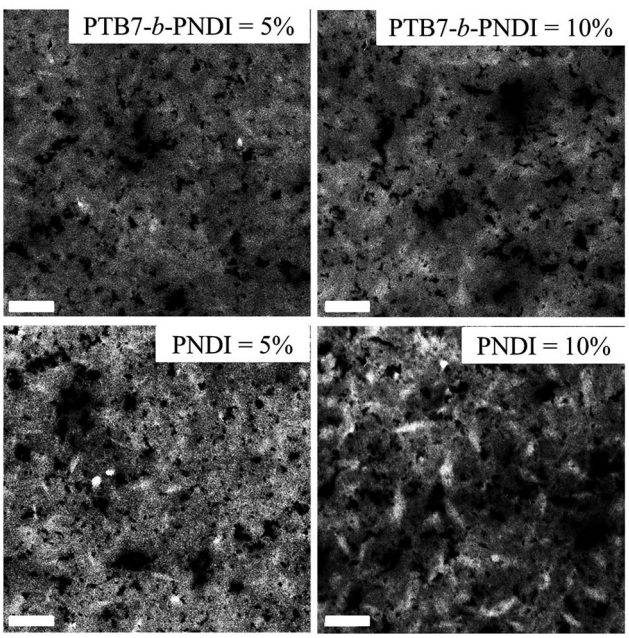

Fig. 6 TEM image of PTB7/PCBM blends with PTB7-*b*-PNDI (top) and PNDI (bottom) as the additive. Scale bar = 200 nm.

domains, gray domains, and white domains. The PCBM is the highest density component, and dark areas indicate the preferential distribution of the PCBM material. Accordingly, we propose that the black domains are rich in PCBM. The relative ordering of the interaction parameters indicates that the strength of segregation between the PNDI and PCBM is stronger than the strength of segregation between the PTB7 and PCBM. Accordingly, it is likely that the PTB7 should distribute preferentially to the space between the PNDI and PCBM (effectively screening the PNDI and PCBM from interacting with one another). Given this explanation, we propose that the gray domains are PTB7 and PCBM intermixed while the white domains are rich in PNDI.

GIWAXS analysis shown in Fig. 7 and in ESI Fig. S11–S14† also supports this interpretation of morphology. Pristine PTB7/PCBM blends exhibit an intense peak along the $q_z = 0.30$ Å^{-1} characteristic from PTB7 and a ring at $q = 1.40$ Å^{-1} from amorphous PCBM. PNDI crystallization is suppressed below 2 wt% PTB7-*b*-PNDI additive, but at 3 wt% PNDI and higher, a diffraction peak at $q = 0.48$ Å^{-1} reflects PNDI crystallization. This suggests enrichment of PNDI into a distinct phase. Similar trends are found for the PNDI homopolymer, except that evidence for crystallization is not observed up to concentrations higher than 3 wt% PNDI additive, suggesting some mixing with PCBM at these low concentrations.

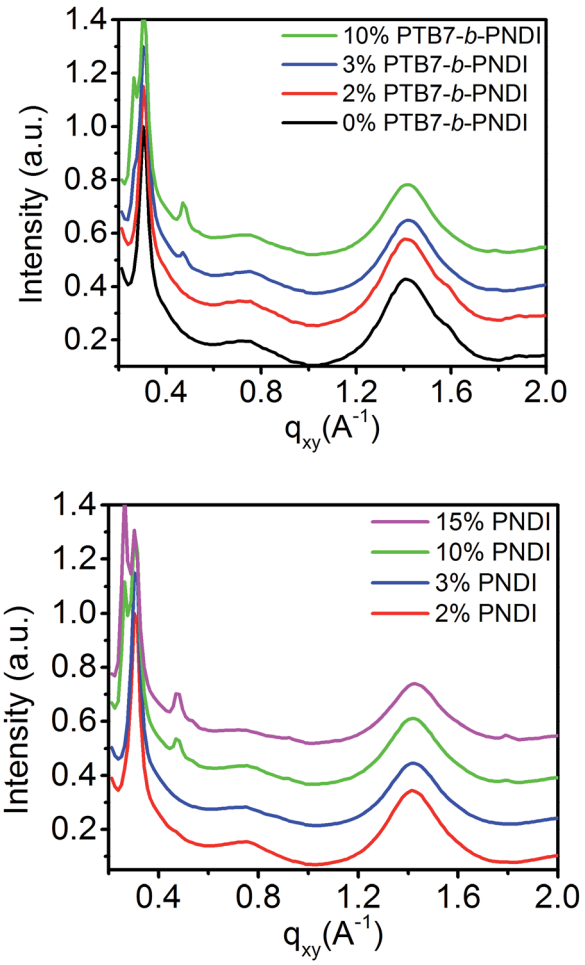

Fig. 7 Linecuts of the grazing incidence wide angle X-ray scattering profile of PTB7/PCBM + PTB7-*b*-PNDI blends and PTB7/PCBM + PNDI blends.

The morphological studies therefore support the picture of phase separated PNDI domains, which supports the hypothesis a parallel-like BHJ OPV with the addition of additives. This also implies that $PCBM_{61}$ mixes preferentially with PTB7 domains. Selective mixing of $PCBM_{61}$ with one polymer of a ternary blend system has been recently observed in a ternary blend system. Hartmeier *et al.* showed that preferential solubility was detrimental to the performance of a ternary blend OPV consisting of two donor polymers, and the authors proposed a guideline for the design of ternary blend OPVs that the miscibility of $PCBM_{61}$ with both polymers should be matched.[54] The present system is comprised of a ternary blend with one donor and one acceptor polymer, and as a result matching $PCBM_{61}$ solubility for both polymers is likely not to be an important design principle. In comparing the V_{OC} trends for BCP and PNDI homopolymer loadings, we propose that the V_{OC} pinning may be sharper for the case of the BCP loading because the PNDI polymer is attached to a PTB7 block. This PTB7 block is likely to shield the PNDI from the PCBM or drive the BCP into the PTB7-rich phase rather than the PCBM-rich domains, which enhances the formation of a parallel-like morphology.

Conclusion

In conclusion, we studied the effect of an all-conjugated block copolymer PTB7-*b*-PNDI in PTB7/PCBM ternary blends solar cells. PTB7-*b*-PNDI was synthesized by sequential Stille polycondensation, in which a low molecular weight PTB7 was used as a macroend-capper. Combination of size-exclusion chromatography, UV-VIS absorption measurements and ^{1}H NMR confirms the success of the sequential polymerization. Small amounts (2 wt%) of BCP lead to significant impact on photovoltaic performance by enhancing open-circuit voltages by 100 mV. We also compared the results with PTB7-*b*-PNDI additives with those with homopolymer PNDI additives, which exhibit a smaller but still significant impact on the V_{OC}. Based on surface energy calculations and morphological analysis through TOF-SIMS and TEM, we conclude that the ternary blend systems studied are consistent with parallel-like OPVs, in which the PNDI forms a distinct acceptor phase. These results point to novel effects with both PNDI and PNDI-*b*-PTB7 additives and suggest that the development of all-conjugated block copolymers with donor and acceptor blocks may be a viable way to tune electronic properties and enhance the performance of BHJ OPVs.

Acknowledgements

J. W. M., L. R. H., and R. V. acknowledge the support of the National Science Foundation (CBET-1264703 and DMR-1352099) and the Welch Foundation for Chemical Research (C-1888) for support of this research. V. G. and D. K. acknowledge support in part by grants from the Robert A. Welch Foundation

(Grant F1599), the National Science Foundation (CBET-1264583), and the US Army Research Office (W911NF-13-1-0396). We acknowledge Krüss for providing support and access to DSA 100 for contact angle measurements. This research used resources of the Advanced Photon Source, a U.S. Department of Energy (DOE) Office of Science User Facility operated for the DOE Office of Science by Argonne National Laboratory under Contract No. DE-AC02-06CH11357. We acknowledge the NSF MRI grant DMR-0923096 for access to TOF-SIMS instrument at the Texas Materials Institute at the University of Texas at Austin.

References

1 N. Li and C. J. Brabec, *Energy Environ. Sci.*, 2015, **8**, 2902–2909.
2 J.-D. Chen, C. Cui, Y.-Q. Li, L. Zhou, Q.-D. Ou, C. Li, Y. Li and J.-X. Tang, *Adv. Mater.*, 2015, **27**, 1035–1041.
3 N. E. Jackson, B. M. Savoie, T. J. Marks, L. X. Chen and M. A. Ratner, *J. Phys. Chem. Lett.*, 2015, **6**, 77–84.
4 K. A. Mazzio and C. K. Luscombe, *Chem. Soc. Rev.*, 2014, **44**, 78–90.
5 F. Liu, W. Zhao, J. R. Tumbleston, C. Wang, Y. Gu, D. Wang, A. L. Briseno, H. Ade and T. P. Russell, *Adv. Energy Mater.*, 2014, **4**, 1301377.
6 Y. Huang, E. J. Kramer, A. J. Heeger and G. C. Bazan, *Chem. Rev.*, 2014, **114**, 7006–7043.
7 H. Chen, Y.-C. Hsiao, B. Hu and M. Dadmun, *Adv. Funct. Mater.*, 2014, **24**, 5129–5136.
8 H. Chen, J. Peet, S. Hu, J. Azoulay, G. Bazan and M. Dadmun, *Adv. Funct. Mater.*, 2013, **24**, 140–150.
9 W. Yin and M. Dadmun, *ACS Nano*, 2011, **5**, 4756–4768.
10 J. T. Rogers, K. Schmidt, M. F. Toney, E. J. Kramer and G. C. Bazan, *Adv. Mater.*, 2011, **23**, 2284–2288.
11 W. Chen, T. Xu, F. He, W. Wang, C. Wang, J. Strzalka, Y. Liu, J. Wen, D. J. Miller, J. Chen, K. Hong, L. Yu and S. B. Darling, *Nano Lett.*, 2011, **11**, 3707–3713.
12 D. Chen, A. Nakahara, D. Wei, D. Nordlund and T. P. Russell, *Nano Lett.*, 2010, **11**, 561–567.
13 G. Li, Y. Yao, H. Yang, V. Shrotriya, G. Yang and Y. Yang, *Adv. Funct. Mater.*, 2007, **17**, 1636–1644.
14 R. A. Segalman, B. McCulloch, S. Kirmayer and J. J. Urban, *Macromolecules*, 2009, **42**, 9205–9216.
15 S. B. Darling, *Energy Environ. Sci.*, 2009, **2**, 1266–1273.
16 I. Botiz and S. B. Darling, *Mater. Today*, 2010, **13**, 42–51.
17 K. Yuan, L. Chen and Y. Chen, *Polym. Int.*, 2014, **63**, 593–606.
18 J. Chen, X. Yu, K. Hong, J. M. Messman, D. L. Pickel, K. Xiao, M. D. Dadmun, J. W. Mays, A. J. Rondinone, B. G. Sumpter and S. M. Kilbey Ii, *J. Mater. Chem.*, 2012, **22**, 13013–13022.
19 Z. Sun, K. Xiao, J. K. Keum, X. Yu, K. Hong, J. Browning, I. N. Ivanov, J. Chen, J. Alonzo, D. Li, B. G. Sumpter, E. A. Payzant, C. M. Rouleau and D. B. Geohegan, *Adv. Mater.*, 2011, **23**, 5529–5535.
20 H. J. Kim, K. Paek, H. Yang, C.-H. Cho, J.-S. Kim, W. Lee and B. J. Kim, *Macromolecules*, 2013, **46**, 8472–8478.
21 R. C. Mulherin, S. Jung, S. Huettner, K. Johnson, P. Kohn, M. Sommer, S. Allard, U. Scherf and N. C. Greenham, *Nano Lett.*, 2011, **11**, 4846–4851.
22 Y.-H. Lee, W.-C. Chen, C.-J. Chiang, K.-C. Kau, W.-S. Liou, Y.-P. Lee, L. Wang and C.-A. Dai, *Nano Energy*, 2015, **13**, 103–116.
23 G. Pandav and V. Ganesan, *Macromolecules*, 2013, **46**, 8334–8344.
24 G. Pandav and V. Ganesan, *J. Chem. Phys.*, 2013, **139**, 214905.
25 D. Kipp, J. Mok, J. Strzalka, S. B. Darling, V. Ganesan and R. Verduzco, *ACS Macro Lett.*, 2015, **4**, 867–871.
26 D. Kipp, O. Wodo, B. Ganapathysubramanian and V. Ganesan, *ACS Macro Lett.*, 2015, **4**, 266–270.
27 L. Yang, H. Zhou, S. C. Price and W. You, *J. Am. Chem. Soc.*, 2012, **134**, 5432–5435.
28 B. M. Savoie, S. Dunaisky, T. J. Marks and M. A. Ratner, *Adv. Energy Mater.*, 2015, **5**, 1400891.
29 A. Yassar, L. Miozzo, R. Gironda and G. Horowitz, *Prog. Polym. Sci.*, 2013, **38**, 791–844.
30 M. J. Robb, S.-Y. Ku and C. J. Hawker, *Adv. Mater.*, 2013, 5686–5700.
31 M. He, F. Qiu and Z. Lin, *J. Mater. Chem.*, 2011, **21**, 17039–17048.
32 Y. Lee and E. D. Gomez, *Macromolecules*, 2015, **48**, 7385–7395.
33 A. Kiriy, V. Senkovskyy and M. Sommer, *Macromol. Rapid Commun.*, 2011, **32**, 1503–1517.
34 I. Osaka and R. D. McCullough, *Acc. Chem. Res.*, 2008, **41**, 1202–1214.
35 K. Okamoto and C. K. Luscombe, *Polym. Chem.*, 2011, **2**, 2424–2434.
36 S. Foster, F. Deledalle, A. Mitani, T. Kimura, K.-B. Kim, T. Okachi, T. Kirchartz, J. Oguma, K. Miyake, J. R. Durrant, S. Doi and J. Nelson, *Adv. Energy Mater.*, 2014, **4**, 1400311.
37 Z. He, C. Zhong, S. Su, M. Xu, H. Wu and Y. Cao, *Nat. Photonics*, 2012, **6**, 591–595.
38 Y. Liang, Z. Xu, J. Xia, S.-T. Tsai, Y. Wu, G. Li, C. Ray and L. Yu, *Adv. Mater.*, 2010, **22**, E135–E138.
39 L. Lu, T. Xu, W. Chen, E. S. Landry and L. Yu, *Nat. Photonics*, 2014, **8**, 716–722.
40 H. Wang, J. Huang, S. Xing and J. Yu, *Org. Electron.*, 2016, **28**, 11–19.
41 L. Lu, M. A. Kelly, W. You and L. Yu, *Nat. Photonics*, 2015, **9**, 491–500.
42 Y. Ohori, T. Hoashi, Y. Yanagi, T. Okukawa, S. Fujii, H. Kataura and Y. Nishioka, *J. Photopolym. Sci. Technol.*, 2014, **27**, 569–575.
43 L. Lu, W. Chen, T. Xu and L. Yu, *Nat. Commun.*, 2015, **6**, 7327.
44 S. A. Mollinger, K. Vandewal and A. Salleo, *Adv. Energy Mater.*, 2015, **5**, 1501335.
45 P. P. Khlyabich, A. E. Rudenko, B. C. Thompson and Y.-L. Loo, *Adv. Funct. Mater.*, 2015, **25**, 5557–5563.
46 R. A. Street, D. Davies, P. P. Khlyabich, B. Burkhart and B. C. Thompson, *J. Am. Chem. Soc.*, 2013, **135**, 986–989.
47 Y.-J. Hwang, T. Earmme, B. A. E. Courtright, F. N. Eberle and S. A. Jenekhe, *J. Am. Chem. Soc.*, 2015, **137**, 4424–4434.
48 W. Lee, C. Lee, H. Yu, D.-J. Kim, C. Wang, H. Y. Woo, J. H. Oh and B. J. Kim, *Adv. Funct. Mater.*, 2016, **26**, 1543–1553.
49 M. M. Durban, P. D. Kazarinoff and C. K. Luscombe, *Macromolecules*, 2010, **43**, 6348–6352.

50 K. Nakano, K. Suzuki, Y. Chen and K. Tajima, *Sci. Rep.*, 2016, **6**, 29529.
51 R. N. S. Sodhi, *Analyst*, 2004, **129**, 483–487.
52 A. Benninghoven, *Angew. Chem., Int. Ed. Engl.*, 1994, **33**, 1023–1043.
53 H. Chou, A. Ismach, R. Ghosh, R. S. Ruoff and A. Dolocan, *Nat. Commun.*, 2015, **6**, 7482.
54 B. F. Hartmeier, M. A. Brady, N. D. Treat, M. J. Robb, T. E. Mates, A. Hexemer, C. Wang, C. J. Hawker, E. J. Kramer and M. L. Chabinyc, *J. Polym. Sci., Part B: Polym. Phys.*, 2015, **54**, 237–246.